Investigation of Dust Shielding Effect of Intrinsic Ergodic Magnetic Field Line Structures in the Peripheral Plasma in the Large Helical Device

M. Shoji[1*], **G. Kawamura**[1], **R. Smirnov**[2], **A. Pigarov**[2], **Y. Tanaka**[3], **S. Masuzaki**[1], **Y. Uesugi**[3], and **the LHD Experiment Group**[1]

[1] National Institute for Fusion Science, National Institutes of Natural Sciences, Oroshi-cho, Toki, Gifu 509-5292 Japan
[2] University of California at San Diego, La Jolla, CA 92093 USA
[3] Kanazawa University, Kakuma, Kanazawa 920-1192 Japan

Received XXXX, revised XXXX, accepted XXXX
Published online XXXX

Key words ergodic layer, dust, long pulse discharge, EMC3-EIRENE, DUSTT

Recent long pulse discharges in the Large Helical Device (LHD) have been interrupted by radiation collapse induced by the emission of dust from the surface of the vacuum vessel and the divertor region. The dust shielding effect by intrinsic ergodic magnetic field line structures (ergodic layer) formed around the main plasma confinement region is investigated using a three-dimensional peripheral plasma fluid code (EMC3-EIRENE) coupled with a dust transport simulation code (DUSTT). Simulations performed in three different magnetic configurations having narrow, medium, and wide ergodic layers show that the wide ergodic layer is not always effective for shielding the main plasma from the dust emission. Optimum operational regimes for controlling the influence of the dust emission on the sustainment of plasma discharges are found by investigating the impurity ion content in the peripheral plasma in various plasma heating powers and plasma densities in the three magnetic configurations.

1 Introduction

The Large Helical Device (LHD) consists of superconducting helical and poloidal coils for forming plasma confinement magnetic field line configurations without the toroidal plasma current, which is advantageous for the sustainment of steady-state plasma discharges [1]. Helically twisted torus plasmas with poloidal/toroidal field periods of ℓ/n=2/10 are produced in the vacuum vessel. The in-axisymmetric magnetic field components produced by the helical coils form intrinsic ergodized magnetic field line structures (ergodic layer) around the main plasma confinement region. The magnetic field lines are bundled into four divertor legs which are deviated from the outermost surface of the ergodic layer [2]. Recent long pulse plasma discharges in LHD have often been interrupted by radiation collapse by impurities (mainly carbon and iron) induced by the emission of dust. Observations with fast framing cameras identified two dust source positions. One is the divertor region and the other is the surface on the vacuum vessel (including helical coil cans). While some long pulse discharges were terminated by carbon dust emission from the divertor region, which were caused by the exfoliation of carbon-rich mixed material deposition layers accumulated near the divertor plates (isotropic graphite) [3-5], some long pulse discharges were interrupted by the iron dust emission from the surface on helical coil cans (stainless steel) just after the appearance of sparks (arcing). An observation with a stereoscopic fast framing camera revealed that iron dust released from the arcing point penetrated the main plasma confinement region to cause the radiation collapse [6].

An impurity transport simulation by a fully three-dimensional peripheral plasma fluid code (EMC3-EIRENE) [7] coupled with a dust transport simulation code (DUSTT) [8-10] shows that the plasma discharges are interrupted by much lower amounts of iron dust emission from the helical coil can compared to that of carbon dust emission from the divertor region [11]. The simulation proves that the effect of the strong plasma flow in the divertor legs prevents the carbon dust from penetrating into the main plasma. On the other hand, the iron dust launched from the helical coil can directly reach the peripheral plasma (the ergodic layer) without the intersection of the divertor legs. It is likely that the iron dust emission from near the main plasma confinement region such as the helical coil can will be a serious obstacle for sustaining long pulse discharges in LHD.

The peripheral plasma formed near the Last Closed Flux Surface (LCFS) in the ergodic layer can effectively prevent the iron dust from penetrating into the main plasma by evaporating the dust due to the plasma heat load

---

* Corresponding author. E-mail: shohji.mamoru@nifs.ac.jp, Phone: +81 572 58 2151, Fax: +81 572 58 2618

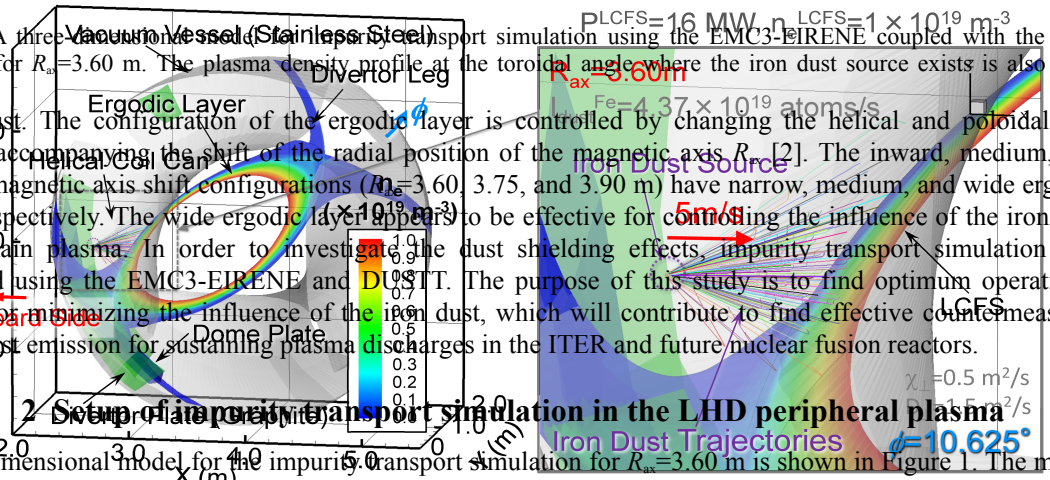

Fig. 1 A three-dimensional model for impurity transport simulation using the EMC3-EIRENE coupled with the DUSTT for R_{ax}=3.60 m. The plasma density profile at the toroidal angle where the iron dust source exists is also shown.

on the dust. The configuration of the ergodic layer is controlled by changing the helical and poloidal coil currents, accompanying the shift of the radial position of the magnetic axis R_{ax} [2]. The inward, medium, and outward magnetic axis shift configurations (R_{ax}=3.60, 3.75, and 3.90 m) have narrow, medium, and wide ergodic layers, respectively. The wide ergodic layer appears to be effective for controlling the influence of the iron dust on the main plasma. In order to investigate the dust shielding effects, impurity transport simulation was performed using the EMC3-EIRENE and DUSTT. The purpose of this study is to find optimum operational regimes for minimizing the influence of the iron dust, which will contribute to find effective countermeasures against dust emission for sustaining plasma discharges in the ITER and future nuclear fusion reactors.

2 Setup of impurity transport simulation in the LHD peripheral plasma

A three-dimensional model for the impurity transport simulation for R_{ax}=3.60 m is shown in Figure 1. The model includes the peripheral plasma (ergodic layer), the divertor legs, the vacuum vessel, the helical coil cans, and the divertor components for one-half of the helical coil pitch angle (18° in toroidal direction) [12, 13]. The typical width of the grid cells in the model is less than 10 mm, but it depends on the radial and poloidal positions of the cells. The surface temperature of the vacuum vessel and the divertor components are set to 300 K and 500 K, respectively. The iron dust source locates on the surface of a helical coil can in the inboard side of the torus which was identified by the observation with the stereoscopic fast framing camera [6]. The poloidal cross-section of a typical plasma density profile in the peripheral plasma at the toroidal angle where the iron dust source exists (a toroidal angle ϕ=10.625°) is also presented. A number of test particles (two million at the maximum), which are representatives of iron dust, are launched from the iron dust source. An enlarged image of the iron dust trajectories is presented in the right figure, showing that most of the iron dust directly reaches the peripheral plasma. The initial dust velocity released from the dust source is set to be 5 m/s which is estimated by the observations with stereoscopic fast framing cameras. The angle of an initial direction of dust emission is randomly chosen from a cosine distribution biased to the direction to the plasma center. The size of a dust (radius) is selected from a Junge distribution in the range from 1 μm to 0.1 mm. This distribution was experimentally found by collecting a number of dust in the vacuum vessel after the past experimental campaigns in LHD [14]. The appropriateness of the Junge distribution in the iron dust emission case has to be verified by a future detailed statistical analysis of dust sizes in full metallic first wall devices in the future. The trajectories of the iron dust released from the dust source are traced by the DUSTT. In this code, it is assumed that the shape of the dust is spherical and that the dust consists of a single element. Thus, iron was adopted as the representative element for stainless steel in which the dominant constituent element is iron. The code provides the profile of the production rate of the neutral iron atoms produced by the evaporation of iron dust. It is assumed that all the neutral iron atoms are ionized at the positions of their production, and impurity production by sputtering on the surface of the vacuum vessel and the divertor plates is not included for the simple calculation. On the dust-surface interactions, dust reflection is not included in the simulation. Steady state background plasma parameter profiles for the DUSTT code are provided by the EMC3-EIRENE in which the perpendicular particle and the thermal diffusion coefficients are assumed to be 0.5 and 1.5 m²/s, respectively. These are typical values in the LHD peripheral plasma obtained by fitting simulations to measurements of the electron density and the

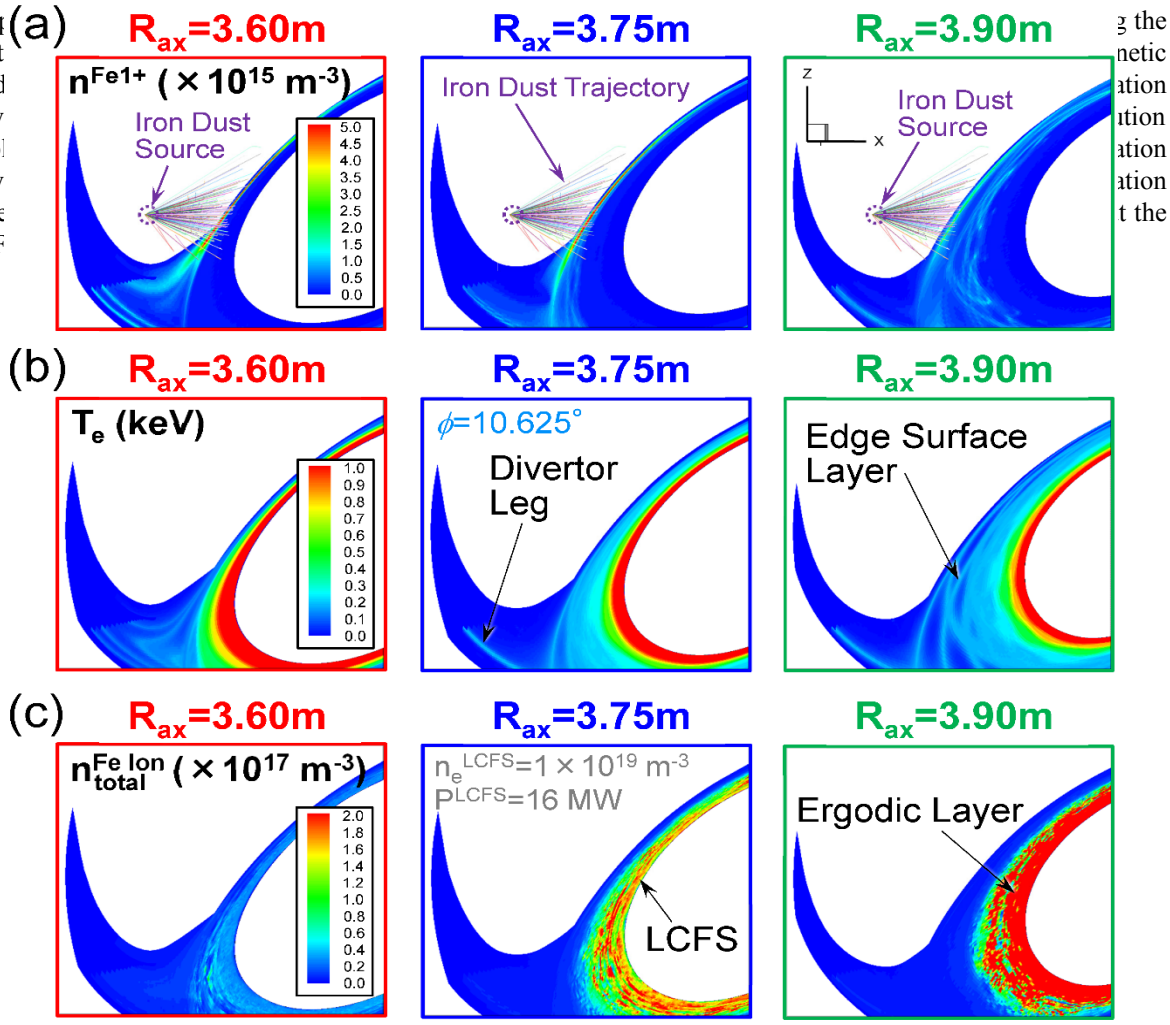

Fig. 2 (a) Poloidal cross sections of the calculated profile of the singly ionized iron ions originated from the iron dust, (b) the electron temperature, and (c) the total iron ion density in the LHD peripheral plasma for the three magnetic configurations (R_{ax}=3.60, 3.75, and 3.90 m) at the toroidal angle where the iron dust source exists (ϕ=10.625°).

3 Impurity transport simulation in three ergodic layer configurations

A constant iron dust emission rate is adopted in the simulation in which a steady state plasma is assumed for the simple calculation. This assumption is justified by the experimental fact that stable plasma discharges are realized (no macroscopic instabilities) in normal operational conditions for long pulse plasma discharges in LHD. However, it has been found that radiative collapse is triggered when the operational condition deviates from the normal conditions, such as a radiative collapse discharge by excessive gas fuelling [16]. The abnormal condition is excluded in the simulation because a converged solution is not obtained in this case. The emission rate of iron dust was set to be 4.37×10^{19} atoms/s, corresponding to the total number of released iron atoms included in the dust per second. Figure 2(a), (b), and (c) illustrate the poloidal cross sections of the calculated profile of the density of singly ionized iron ions originated from the iron dust with typical dust trajectories, the electron temperature, and the total iron ion density (including those with all ionization stages) at the toroidal angle where the iron dust source exists (ϕ=10.625°), respectively. In the simulations, the plasma heating power and the plasma density at the LCFS are 16 MW and 1×10^{19} m^{-3}, respectively. The figure shows that singly ionized iron ions are localized in the outermost surface of the ergodic layer near the dust source. It is very interesting that the profile of the total iron ion density for the inward magnetic axis configuration (R_{ax}=3.60 m) is significantly lower than that in the other two magnetic configurations (R_{ax}=3.75 and 3.90 m).

It is well known that the impurity ion density in the peripheral plasma is determined by the balance between the thermal force F_{therm} and the friction force F_{fric} on the impurity ions along the magnetic field lines [17]. While, the thermal force pulls up the impurity ions to the upstream side of the magnetic field lines (to the main plasma), the friction force exhausts the impurity ions to the downstream side (to the divertor region). Figure 3(a) depicts the poloidal cross sections of the profile of the production rate of the neutral iron atoms generated by the evaporation

of the dust and Figure 3(b) shows the force balance (F_{fric}- F_{therm}) in the three magnetic configurations. As indicated in Figure 3(a), the position where neutral iron atoms are produced (iron dust evaporation zone) locates in the outermost surface of the ergodic layer. The simulations of the profile of the force balance presented in Figure 3(b) clearly show that in the inward magnetic axis shift configuration (R_{ax}=3.60 m), the friction force dominant area (shown as red) is clearly separated from the thermal force dominant area (shown as blue). On the other hand, in the medium and outward magnetic axis shift configurations (R_{ax}=3.75 and 3.90 m), the friction force dominant areas are alternately and complexly mixed with the thermal force dominant areas.
In the inward magnetic axis shift configuration, the iron dust evaporation zone exists in the friction force dominant area, which is the main reason for the low total iron ion density in the ergodic layer (the left image in Figure 2(c)). On the other hand, in the outward magnetic axis shift configuration, the iron dust evaporation zone partly locates on the thermal force dominant areas in the edge surface layer (shown as blue), which explains the high iron ion density (the right image in Figure 2(c)). The simulations clearly prove that the wide ergodic layer itself is not always effective for controlling the impurity ion density in the LHD peripheral plasma.

4 Investigation of optimum operational regimes for controlling the impurity ion content in the peripheral plasma

Finding the optimum operational regimes for controlling the influence of the iron dust emission on the peripheral plasma is essential for sustaining long pulse discharges in LHD. The total iron ion content $Q^{Fe\ ion}$ in the peripheral plasma (including the ergodic layer and the divertor legs) is adopted as an indicator of the iron dust shielding effect. The total iron ion content in the three magnetic configurations was investigated in various plasma heating powers and the plasma densities at the LCFS (P^{LCFS} and n_e^{LCFS}). The total iron ion content is scanned in the ranges of the plasma heating power and the plasma density (1 MW$\leq P^{LCFS} \leq$16 MW and 1×10^{19} m$^{-3}\leq n_e^{LCFS} \leq 8\times10^{19}$ m^{-3}).

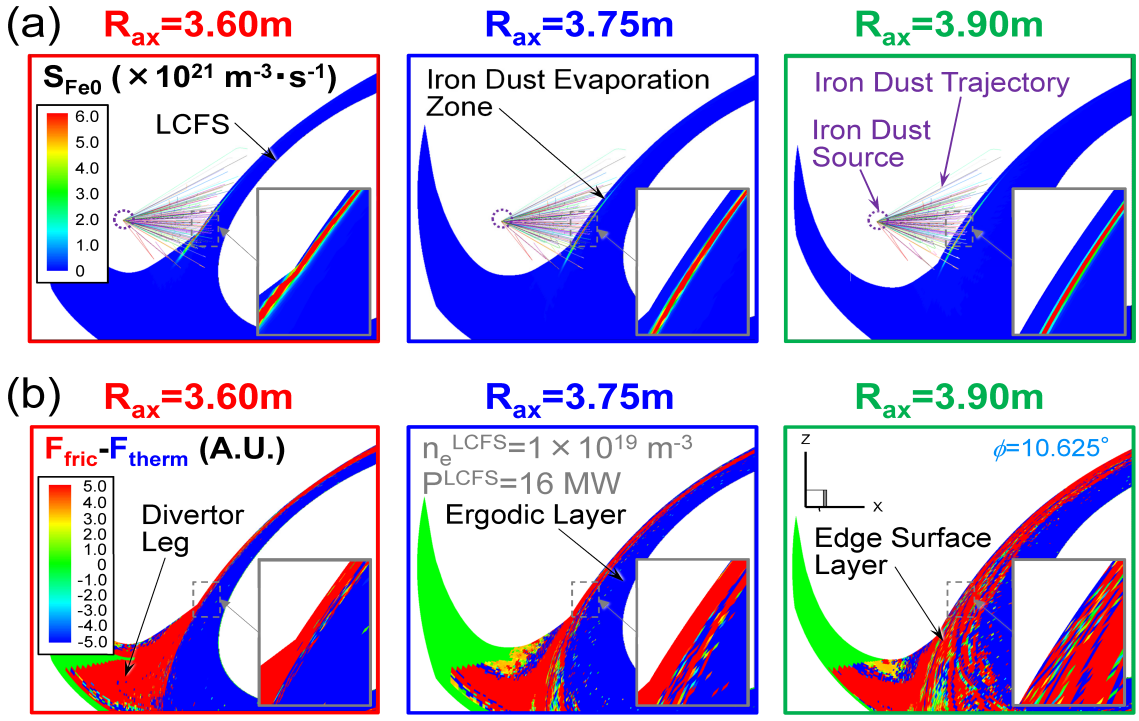

Fig. 3 Poloidal cross sections of the profile of the production rate of the neutral iron atoms generated by the evaporation of the iron dust (a), and the balance between the thermal force and the friction force on the iron ions in the three magnetic configurations (R_{ax}=3.60, 3.75, and 3.90 m) (b).

The parameter $Q^{Fe\ ion}$ is calculated by summing the value $n_{i,j,k}^{Fe\ ion}\times V_{i,j,k}$ in the model for the simulation. Here, $n_{i,j,k}^{Fe\ ion}$ and $V_{i,j,k}$ are the sum of iron ion densities with all ionization stages and the grid cell volume at the position assigned by the radial, poloidal, and toroidal index numbers i, j, and k in the model, respectively. Figure 4(a), (b), and (c) depict the two-dimensional contour plots of the total iron ion content in the peripheral plasma in the three magnetic configurations. Areas painted over in white indicate the parameter ranges where a converged solution is not obtained. In this case, the electron temperature significantly drops and the radiation power induced by iron ions drastically increases. This situation indicates that the plasma is not stably sustained because of the insufficient plasma heating power induced by radiation cooling due to the iron dust.

The figure indicates that the parameter condition for the optimum operational regimes is quite different in between R_{ax}=3.60 and 3.90 m. In the inward magnetic axis shift configuration (R_{ax}=3.60 m), there are two choices for favorable plasma discharges with reduced iron ion content. Plasma discharge operation with high plasma heating powers (P^{LCFS}≥12 MW) and a quite low plasma density (n_e^{LCFS}=1×10^{19} m^{-3}) (indicated as "A" in figure 4(a)) gives a low iron ion content, and operation with the high plasma heating powers and high plasma densities (n_e^{LCFS}>6×10^{19} m^{-3}) (as "B") is also desirable. On the other hand, in the outward magnetic axis shift configuration (R_{ax}=3.90 m), operation with the high plasma heating powers and the low plasma density (shown as "C" in figure 4(c)) brings catastrophic increase in the iron ion content, which is not appropriate for stable steady-state plasma discharges. Operation with the high plasma heating powers and relatively higher plasma densities (n_e^{LCFS}>6×10^{19} m^{-3}) (as "D") is effective for diminishing the impurity ion content. The simulation for R_{ax}=3.75 m presents an intermediate trend between those for R_{ax}=3.60 and 3.90 m. In this magnetic configuration (R_{ax}=3.75 m), favourable operational conditions for shielding the dust are those with the high plasma heating powers and higher plasma densities (denoted as "E" in figure 4(b)). The reason for the quite different parameter condition for the optimum operational regime in the two magnetic configurations (R_{ax}=3.60 and 3.90 m) is attributed to the contrasting magnetic field line structures in the outermost surface of the ergodic layer, namely, the different spatial distribution of the friction force dominant areas and the thermal force dominant areas in the ergodic layer.

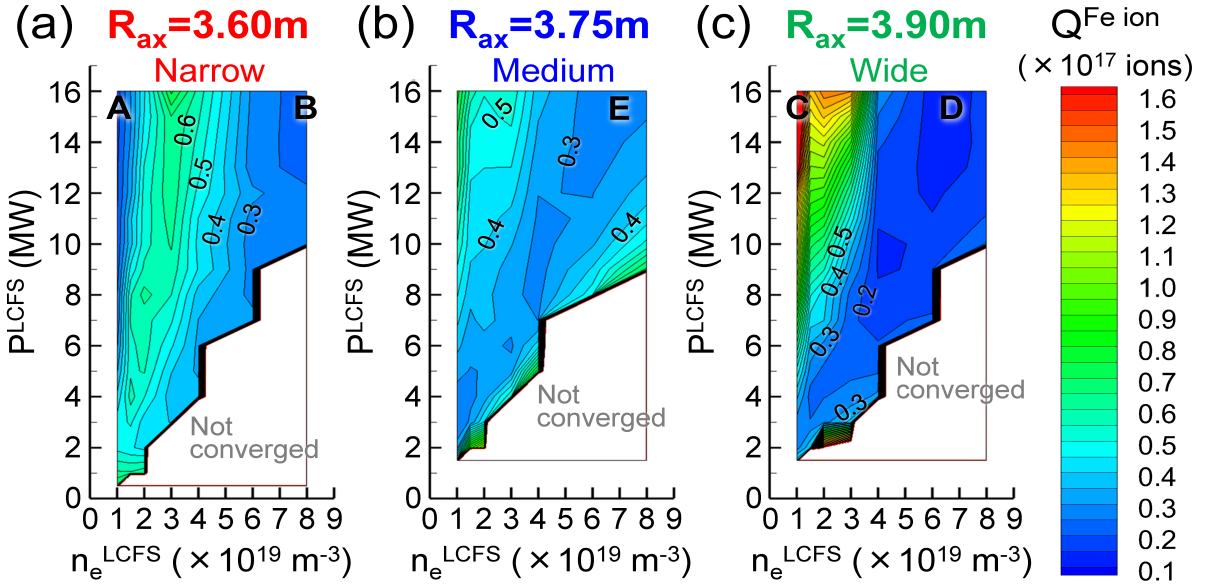

Fig. 4 Contour plots of the total iron ion content in the three magnetic configurations (R_{ax}=3.60, 3.75, and 3.90 m) in the two-dimensional ranges of the plasma densities (n_e^{LCFS}) and the plasma heating powers (P^{LCFS}) at the LCFS.

In the inward magnetic axis shift configuration (R_{ax}=3.60 m), while the friction force dominant area is formed in the outermost surface of the narrow ergodic layer, the thermal force dominant area (shown as blue) exists in the inside of the outermost surface (as depicted in the left image in Figure 3(b)). The iron dust evaporation zone locates in the outermost surface for the high heating powers with the low plasma density because of the high heat load on the dust there as shown in the left image in Figure 3(a). Simulations show that for lower plasma heating powers or for higher plasma densities, the position of the evaporation zone approach the LCFS in the inner area of the ergodic layer because of the insufficient heat load on the dust (the evaporation rate of iron atoms from the dust is more sensitive to the plasma temperature than the plasma density). When the plasma density is higher than 2×10^{19} m^{-3} with the high plasma heating powers (P^{LCFS}≥12 MW), the iron ion content mainly depends on the magnitude of the thermal force because the iron dust evaporation zone locates in the thermal force dominant area in the inside of the outermost surface. The high iron ion content in moderate plasma densities (n_e^{LCFS}=3~4×10^{19} m^{-3}) with the high plasma heating powers is explained by the enhanced thermal force driven by the steep plasma temperature gradient in the ergodic layer due to the high plasma temperature near the LCFS. The low iron ion content for the higher plasma densities (n_e^{LCFS}>6×10^{19} m^{-3}) with the high plasma heating powers is due to the reduced thermal force by the low temperature gradient. It should be noted that the enhanced friction force due to the higher plasma densities in the ergodic layer also contributes to the low iron ion content.

On the other hand, in the outward magnetic axis shift configuration (R_{ax}=3.90 m) the iron dust evaporation zone partly locates in thermal force dominant areas on the edge surface layers in the wide ergodic layer (as shown in the right figures in Figure 3(a) and (b)). The simulation shows that this situation is not changed in various plasma heating power and plasma density conditions, indicating that the iron ion content is determined by the

magnitude of the thermal force in the edge surface layers. Thus, the main reason for the significant increase in the iron ion content for the high plasma heating powers with the quite low plasma density ($n_e^{LCFS}=1\times10^{19}$ m^{-3}) is the enhanced temperature gradient by the high plasma temperature near the LCFS. This interpretation explains the low iron ion content for the high plasma heating power with the higher plasma densities ($n_e^{LCFS}>6\times10^{19}$ m^{-3}) because of the low temperature gradient. As well as the condition in the inward magnetic axis configuration, the enhanced friction force promotes the low iron ion content in the higher plasma densities in this magnetic configuration.

5 Summary

The iron dust shielding effect by the ergodic layer intrinsically formed in the LHD peripheral plasma was investigated using a three-dimensional peripheral plasma fluid code (EMC3-EIRENE) coupled with a dust transport simulation code (DUSTT) in the three magnetic configurations having narrow, medium, and wide ergodic layers. The simulation proves that the wide ergodic layer is not always effective for controlling the iron ion content in the peripheral plasma. The simulations in various plasma heating powers and plasma densities in the three magnetic configurations found optimum operational regimes for reducing the iron ion content. In the narrow ergodic layer configuration (R_{ax}=3.60 m), there are two choices for favorable operational regimes. One is plasma discharges with high heating powers ($P^{LCFS}\geq$12 MW) and a quite low plasma density ($n_e^{LCFS}=1\times10^{19}$ m^{-3}) in which a friction force dominant area formed in the outermost surface of the ergodic layer shields the iron dust. The other candidate is plasma discharge operation with high plasma heating powers and high plasma densities ($n_e^{LCFS}>6\times10^{19}$ m^{-3}) in which the reduced thermal force on the iron ions in the ergodic layer decreases the iron ion content. On the other hand, in the wide ergodic layer configuration (R_{ax}=3.90 m), operation with the high plasma heating powers with the high plasma densities is the only choice for controlling the iron ion content. The medium ergodic layer configuration (R_{ax}=3.75 m) has an intermediate trend on the two parameters (P^{LCFS} and n_e^{LCFS}) between those for the above two magnetic configurations. These simulations will contribute to the sustainment of stable plasma discharges by minimizing the influence of the iron dust emission on LHD plasmas.

Acknowledgements This work is supported by a NIFS budget (NIFSULPP015) and is performed with the support and under the auspices of the NIFS Collaboration Research program (NIFS12KNXN236). One of the authors (M. S.) would like to thank Y. Feng for permission to use the EMC3-EIRENE. He is also grateful for the computational resources of the LHD numerical analysis server and the plasma simulator in NIFS. This work is also supported by JSPS KAKENHI Grant Numbers 16H04619 and the U.S. DOE Grant DE-FG02-06ER54852.

References

[1] A. Komori et al., Fusion Sci. and Technol. **58**, 1 (2010).
[2] N. Ohyabu et al., Nucl. Fusion **34**, 387 (1994).
[3] M. Shoji et al., Nucl. Fusion **55**, 053014 (2015).
[4] Y. Yoshimura et al., Nucl. Fusion **56**, 046005 (2016).
[5] M. Tokitani et al., J. Nucl. Mater. **463**, 91 (2015).
[6] M. Shoji et al., Plasma and Fusion Res. **11**, 2402056 (2016).
[7] Y. Feng et al., Plasma Phys. Control. Fusion **44**, 611 (2001).
[8] A. Yu Pigarov et al., J. Nucl. Mater. **363-365**, 216 (2007).
[9] R. D. Smirnov et al., Plasma Phys. Control Fusion **49**, 347 (2007).
[10] Y. Tanaka et al., J. Nucl. Mater. **415**, S1106 (2011).
[11] M. Shoji et al., Nuclear Materials and Energy **12**, 779 (2017).
[12] G. Kawamura et al., Contrib. Plasma Phys. **54**, 437 (2014).
[13] M. Shoji et al., Contrib. Plasma Phys. **56**, 651 (2016).
[14] K. Koga et al., Plasma and Fusion Res. **4**, 034 (2009).
[15] The ADAS User Manual (version 2.6) http://adas.phys.strath.ac.uk/ (2004).
[16] B. J. Peterson et al., Phys. Plasmas. **8**, 3861 (2001).
[17] M. Kobayashi et al., Contrib. Plasma Phys. **48**, 255 (2008).